NUMERICAL SIMULATION OF INDOOR AIR DISTRIBUTION AND WALL HEAT STORAGE UNDER ACCIDENT CONDITIOHS IN A MAIN CONTROL ROOM

Huikang Cai[1], Shuaijie Sha[2], Tai Xu[3], Yannan Li[4], Hanzhong Tao[5,*]

School of energy science and engineering, Nanjing Tech University, Jiangsu 211816, China

[*] Corresponding author; taohanzhong@njtech.edu.cn

Abstract:

The main control room serves as a refuge for staff in a nuclear power plant in the event of an accident. To determine whether the control room can meet habitability requirements under accident conditions, this study utilized computational fluid dynamics methods to establish a habitability model of the main control room under such conditions. The changing trends of temperature and velocity near personnel were analyzed. The numerical results indicate that the building envelope significantly contributes to reducing the indoor temperature. The average wall temperature measured at 72 hours was 27°C, with an average temperature increase of 4°C. The highest average ambient temperature in the main control room occurred at 24 hours. At this time, the indoor ambient temperature reached approximately 34.62°C, with a temperature increase of 11.62°C, while the wind speed near the personnel remained below 0.2m/s, meeting habitability requirements for personnel under extreme conditions.

Keywords: *CFD simulation; habitability of main control room; heat storage of envelope; nuclear power plant*

1. Introduction

As an important form of energy, nuclear energy has the characteristics of safety, cleanness and economy, and can be used on a large scale [1]. However, the Fukushima nuclear accident [2] in Japan has made people worried about the safety of nuclear power. This nuclear crisis was the largest nuclear accident after the Chernobyl nuclear disaster on April 26, 1986 [3], resulting in serious casualties of nuclear power plant staff [4]. Since then, people have paid increased attention to the safety of nuclear power.

To reduce the number of casualties during accidents, it is necessary to establish a safe and healthy environment for the staff. This temporary shelter can be the main control room (MCR), which is the main control center of the whole nuclear power plant (NPP). In the event of a nuclear accident, the MCR protects the occupants from the harmful effects of radioactive substances, explosive substances and toxic gases with high radiation levels [5], [6] due to the isolated air purification and ventilation system[7]. The shutdown of the NPP is a complex process, therefore it leads to a long-term, usually 72-hour occupancy period in the MCR[8]. The indoor air temperature will increase as a result of the internal heat loads generated by the human bodies and technical equipment[9]. If the air temperature in the MCR exceed the upper limit of human heat tolerance (35°C wet-bulb temperature [10], [11]), it will pose a danger to the safety of employees. To ensure and maintain the acceptable thermal environmental conditions for indoor personnel to survive, measures must be taken in the MCR to maintain the acceptable an indoor thermal condition [12].

Room temperature range has a significant impact on indoor environmental quality. Under normal operating conditions, the allowable temperature range can be maintained using the central air conditioning system of the MCR. However, if an accident occurs, the air conditioning system cannot operate in the event of power failure. To solve this problem, the AP1000 NPP's passive safety system has been developed to ensure the fundamental functions using only natural effects, e.g. by compressed air expansion [13]. Some research conducted on passive refrigeration in the MCR of NPP. Li et al. studied the use of isentropic expansion of compressed air for refrigeration, and the results show that this method can meet the requirements of occupancy in the MCR [8]. Jia et al. studied the ice storage bin of the coal mine shelter, tested the effective cooling time of the system, and provided help for the temperature control of the shelter [14]. Wang et al. proposed a new compressed air refrigeration system, which reduces the operation cost of the system [15]. Siddiqui et al. conducted an economic analysis of the hybrid storage absorption refrigeration cycle system [16].

In addition, the cold storage technology of concrete structures [17] can significantly reduce the indoor temperature of the MCR. The internal heat gain result difference between the walls and the room air temperature. Due to the heat transfer trough the walls and the thermal storage reinforced concrete structures; the indoor air temperature remains within the acceptable limits. are used to store heat, to discharge the indoor heat dissipation and maintain the indoor temperature. Huang et al. studied the dynamic thermal process of the concrete ceiling with fins in the MCR, and maintained the thermal habitability of the MCR through the ceiling made of concrete [18]. Al-Rukaibawi et al. numerically studied the influence of envelope structure on overheating risk in summer, and analyzed the overheating problem and thermal comfort of four envelope structures [19]. Gollapudi et al. numerically analyzed the heat transfer performance of envelope with horizontal fins [20].

In summary, indoor air temperature is an important reference factor. For NPPs, before implementing various passive cooling facilities in the design and layout of the main control room that operate naturally without relying on electricity, it is necessary to investigate whether habitability indoor can be maintained solely through its own enclosed structure for up to 72 hours. However, there is little research on this aspect at present. Therefore, this study aims to fill this gap by establishing a finite volume computational fluid dynamics (CFD) program. Through the CFD simulation technology, we can obtain detailed distributions of the indoor thermal environment and provide a reference for future optimization. Based on a small NPP, the heat storage of the MCR wall envelope is considered, and a ventilation system for precooling air supply is applied in this study. The system primarily uses the compressed air tanks to spray low-temperature fresh air and mix it with indoor return air to reduce the supply air temperature to a certain extent. Meanwhile, RNG k-ε turbulence model and models for equipment with certain heating power and human body heat generation are established. Finally, the indoor airflow field and temperature field of the MCR under accident conditions are analyzed.

2. Numerical simulation

2.1. Physical models

A three-dimensional model of the same size (17.55m×14.15m×4.1m) as the interior of the MCR was established. In this study, the heat storage effect of the upper and lower walls was not considered, as they are exposed to high-temperature environments. Instead, the surfaces of the upper and lower walls were treated as adiabatic walls. The wall surrounding the MCR is shared with other rooms on the

same floor, which means that the temperature of the wall on the MCR side can be affected by heat dissipation

from other rooms. To accurately capture this effect, only half thickness of the wall was used in the model, with a thickness of 0.4m. Fig.1 shows the established 3D model. In this model, the MCR consists of walls, equipment, ventilation ducts and personnel. The equipment includes console, screen, and computer desks. The human body model was established based on "Chinese Adult Human Body Dimensions", as shown in Fig.1 (a) and (b). Human breathing is considered in this paper, and the breathing area is 0.04m×0.02m rectangle. In this model, 11 people were divided into 3 rows, the first 2 rows are in a sitting position and the 3rd row is in a standing position.

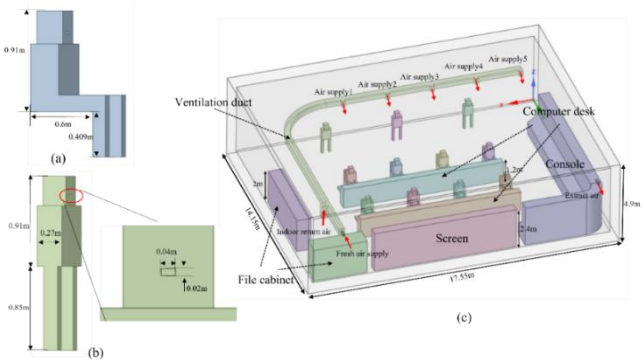

Fig.1. (a) People in sitting position; (b) People in standing position; (c) Three-dimensional model of the MCR

The main control room is preset with fresh air to ensure the survival of personnel for 72 hours, which is stored in the compressed air tank. When an accident occurred, fresh air was ejected from the compressed air tank into the ventilation ducts and mixed with the indoor return air to reduce the temperature of the supply air. There are five air supply outlets in the MCR. The center height of the air supply outlet is 3 meters, and the air supply direction is at an angle of 0° with the horizontal direction. Considering the penetration of indoor air, an outlet is set at the upper end of the side wall.

Equipment and human models are shown in Fig. 1 (c), in which the heating area of the large screen is 44.8 m^2, the heating area of the console is 82.41 m^2, and the heating area of the computer desk is 71.28 m^2. The cross-sectional area of the fresh air inlet is 0.01 m^2, the cross-sectional area of the supply air is 0.064 m^2, and the cross-sectional area of the return air is 0.1024 m^2. To reduce the grid and save computing resources, the surface without thickness was used to build equipment and personnel.

2.2. Monitoring planes and lines

For further research, monitoring planes and monitoring lines are set in the MCR to obtain the changes of indoor flow pattern and temperature field. The height of people sitting indoors is about 1.3m, and the height of people standing is about 1.8m. To study the indoor habitability and capture the flow field and temperature field at the neck and ankle of personnel, monitoring planes P1, P2 and P3 and monitoring lines L1-L12 are set in the occupied area of personnel. The monitoring plans P1 (y=1.6m), P2 (y=5.3m) and P3 (y=8.3m) respectively pass through three rows of people, and the monitoring lines L1-L12 is distributed in the habitable area by people, as shown in Fig. 2 (a) and (b). To study the flow field and thermal conditions in the habitable area under different personnel distributions, the habitable area with a height of 0-2.2m is drawn, as shown in Fig. 2 (c).

2.3. Boundary conditions

To evaluate the habitability of the MCR under accident conditions, this paper adopts the numerical simulation method. Table 1 shows the heat dissipation of each heat source in MCR under accident conditions. According to the data in Table 1, under accident conditions, the ventilation system is closed or isolated to prevent pollutants from entering MCR. The equipment remains in operation for 24 hours to perform the safe shutdown task and generates heat. The total heat dissipation in MCR at this stage is 12kW. After 24 hours, the equipment shuts down after performing the safe shutdown task. During this period, the total heat dissipation of MCR is 1kW.

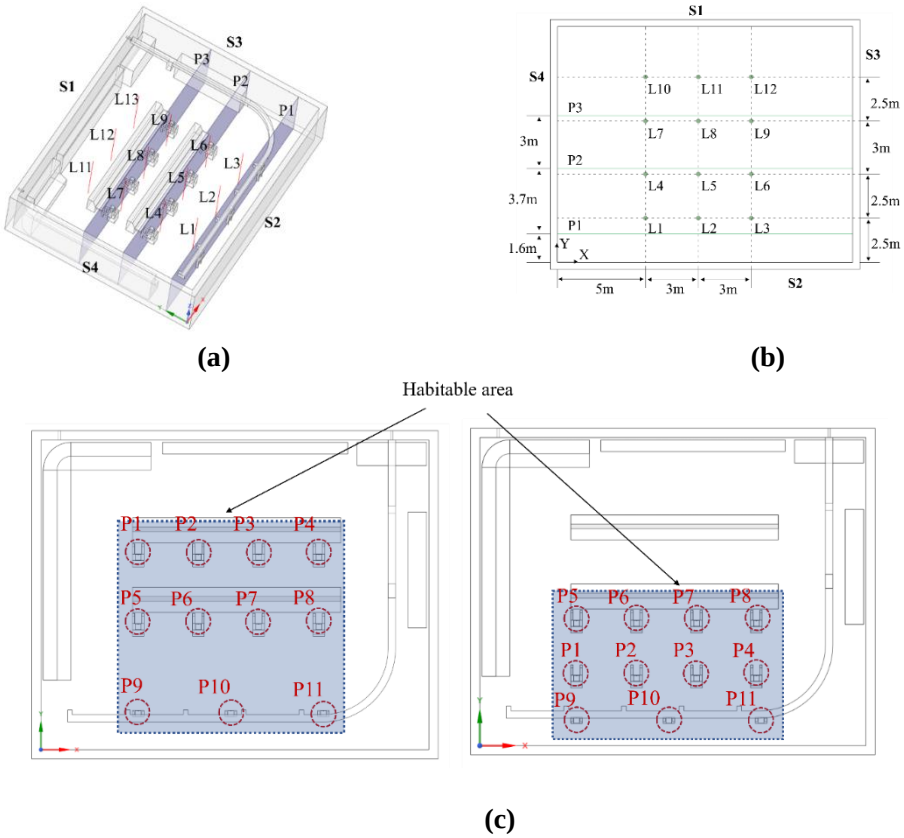

Fig. 2. Schematic view of monitoring plans and lines; (a) 3D schematic view, (b) Details of monitoring plans and lines, (c) Location of the habitable area of the MCR in case1 and case3

Table 1 Heat dissipation of heat source in main control room

	Heat source area/m^2	Heat dissipation/kW	
		0-24h	24-72h
Screen	44.8	3	0
People	24.54	1	1
Console	82.41	6	0
Computer desk	721.28	2	0
Total heat dissipation		12	1

Heat gain refers to the additional heat absorbed by a building or system, resulting in an increase in indoor temperature. Heat gain is an important consideration in architectural engineering and HVAC design because it affects indoor temperatures and the load on HVAC systems. In this paper, indoor heat gain includes equipment heat dissipation and metabolic heat production from indoor personnel. When a person sits quietly in the MCR, the metabolic rate of the human body is 1 met and is equal to

91W total heat gain. The equipment operates normally in the first 24 hours, so the surface heat flow is defined as 66.96W/m^2, 72.81 W/m^2 and 28.06W/m^2 for the screen, console, and computer desk respectively. After 24 hours, the equipment stopped running and the surface heat flow changed to 0W/m^2. Meanwhile, the non-slip condition was imposed on all solid walls.

The velocity inlet boundary condition is set at the fresh air supply. The temperature of fresh air provided is $15°C$, and the airflow is 113m^3/h. The turbulence intensity and hydraulic diameter of the inlet are calculated by the following formulas:

$$d = 4A/S \quad (1)$$

$$Re = vd/\mu \quad (2)$$

$$I = 0.16Re^{-0.125} \quad (3)$$

Pressure outlets serve as the boundary conditions for the outlet, while indoor return air and the five air supply outlets are designated as fan boundaries. Fan boundaries require specification of pressure drop and direction to determine fluid flow and orientation. Specifically, the pressure jump for indoor return air is set to 17Pa, and for the five air supply outlets, the pressure jumps are individually configured as 7.5Pa, 6.5Pa, 6Pa, 4.5Pa, and 3.5Pa. Their average direction aligns with the positive y-axis. The indoor return air flow rate is set at 1020m³/h, with the zone-average direction aligned to the positive z-axis, as illustrated in Fig.1(c). The indoor inlet air velocity is 3.14m/s, and the temperature is maintained at 288K.

Most of the enclosure structures of the MCR and the control equipment room are composed of reinforced concrete, and the proportion of glass windows in the MCR enclosure structure is small. For the convenience of calculation, they are simplified to reinforced concrete. Non-heat-source objects such as chairs and filing cabinets are set as wood, and the physical parameters of the human body and water are approximated. The physical parameters of each material are shown in Table 2.

Table 2 Material properties

	Density (kg/m^3)	Specific heat capacity (J/kg K)	Thermal conductivity (W/m K)
Wall	2650	960	1.74
Chair and file cabinet	700	2310	0.17
people	1048	4200	0.43

2.4. Case description

The air domain of the MCR is 16.75m long, 13.35m wide and 4.1m high. The actual thickness of the wall is 0.8m. Due to the high temperature environment outside of the MCR, the theoretical effective thermal storage thickness of the wall is 0.4m. The impact of walls, equipment, and personnel on the thermal environment of the MCR are analyzed by using different cases. Case1 is the actual working condition, and in the actual situation, the upper and lower floors of the MCR are in high temperature environment, so heat storage of ceiling and floor are not considered; Case2 is the ideal working condition, that is, the heat storage of ceiling and floor is considered; to study the impact of personnel position on the thermal environment of the MCR, case 3 moves the first rows of personnel away the equipment based on case 1.

2.5. Numerical details and grid independence

The model was meshed, and a structured mesh dominated by hexahedron was generated to improve the mesh quality. Grid encryption was carried out for the entrance, exit, human body, and equipment departments to ensure the accuracy of the calculation results. The main advantage of structured grid was that each cell has adjacent nodes. Therefore, compared with tetrahedral mesh, it can better calculate the gradient and reduce the number of meshes. The finite volume numerical method was used to simulate the temperature and airflow distribution in the room, and this method was used for the diffusion and source terms. A gravitational acceleration along the negative direction of the z-axis was set, the pressure was discretized in a body-weighted format, and the energy and momentum were discretized in a second-order upwind format. To analyze the reliability of the obtained data, a convergence criterion was established, which was less than 10^{-4} for convergence variables except energy, and less than 10^{-8} for energy. The time step is 30s.

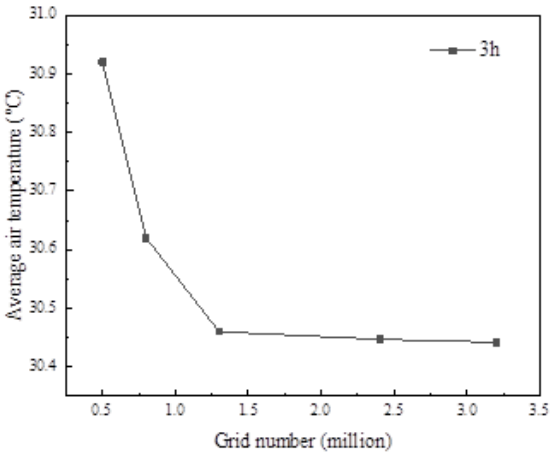

Fig3. Grid-independence verification

When dividing the grid, different parameters were set to change the size and sparsity of the grid. The grid number of the grid model was divided into 0.5×10^6, 0.8×10^6, 1.3×10^6, 2.4×10^6 and 3.2×10^6, respectively. Set the same boundary conditions to simulate different grid numbers under no stationary. Using average air temperature parameters to evaluate the influence of grid size on simulation quality. As can be seen from Fig.3, when the number of grids is 1.3×10^6, the average air temperature began to tend to a fixed value, and the grid became independent. Considering the main computing resources available, the model with 2.4×10^6 grids is selected for calculation.

3. Results and discussions

3.1. Model validation

To verify the reliability of the numerical model for temperature distribution in the MCR, the results obtained from the numerical simulation were compared with the data provided by D. Palanisamy[22]. Usually, the temperature distribution in the room can be well modelled by CFD. The validation model used is a control room measuring 3m in length, 6.1m in width, and 2.4m in height. The verification results are shown in the Fig.4, indicating an average error of simulated data is 0.74% and a maximum error of 1.28% for the simulated data. The average error for experimental measurement is 4.13%, with the maximum error of

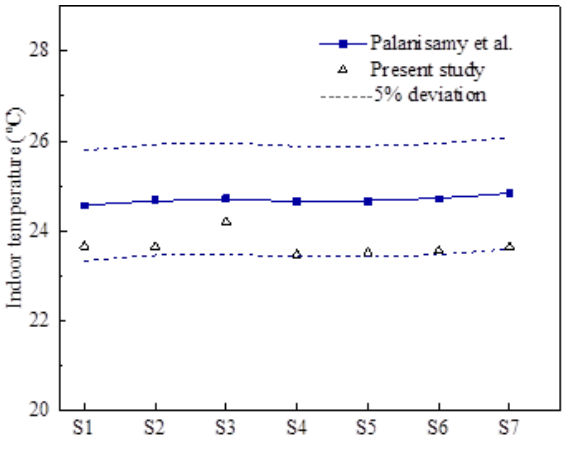

Fig.4. Temperature distribution verification results

4.8%. These results demonstrate good agreement between that the numerical simulation results and experimental data.

3.2. Thermal storage effect of building envelope

3.2.1 Influence of walls on indoor thermal environment

Firstly, for the case of no wall thermal storage (the ability of wall materials to absorb, store, and release heat), the calculation results show that the indoor air temperature reaches 36.8°C at 0.5 hours. It can be concluded that this condition cannot meet the livability requirements of the main control room. Then, the dynamic changes of the average MCR air temperature and wall temperature over time were studied for case 1 and case 2. Fig.5 shows the dynamic changes of the average MCR air temperature over time for the two cases. It can be observed that the air temperature in both case 1 and case 2 rapidly increases in the first 0.5 hours. For case 1, the temperature rises at a rate of 5.35°C/h and 0.18°C/min in the first 0.5 hours, and significantly slows down to 0.27°C/h from 0.5 to 24 hours, due to the delayed thermal storage effect of the wall. When the NPP experiences a power outage for 24 hours during the accident, the MCR average air temperature reaches its peak, and the results show that the air temperature for case 1 at this time is 34.62°C. After the equipment runs for 24 hours to complete the shutdown task and stops running, the average indoor air temperature begins to decrease. From Fig.5, there is a sudden temperature drop process after the equipment stops running, and then the cooling rate gradually decreases and eventually stabilizes. In the sudden drop process, the average air temperature in case 1 decreases from 34.62°C at 24 hours to 29.91°C at 25 hours, with a temperature decrease of 4.71°C. The average temperature stabilizes at 27.61°C at 48 hours.

Case 2 is the ideal condition, considering the thermal storage effect of the ceiling and floor based on case 1. It can be seen from the figure that the trend of the indoor average air temperature with time for case 2 is like that of case 1. In the first 0.5 hours of equipment operation, the air temperature also experiences a sudden temperature rise process. The indoor air temperature of MCR rises by 2.65°C in the first 0.5 hours, with a temperature rise rate of 5.3°C/h. From 0.5 to 24 hours, the temperature rise rate decreases to 0.18 °C/h. The indoor air temperature reaches its highest point at 24 hours, which is 27.72°C. After the equipment stops running for one hour, the indoor air temperature decreases by 1.12°C, and when the equipment stops running for 24 hours, the indoor temperature stabilizes at 24.79°C. The thermal storage of the envelope structure plays a significant role in reducing indoor air temperature and has an important impact on the livability of the MCR.

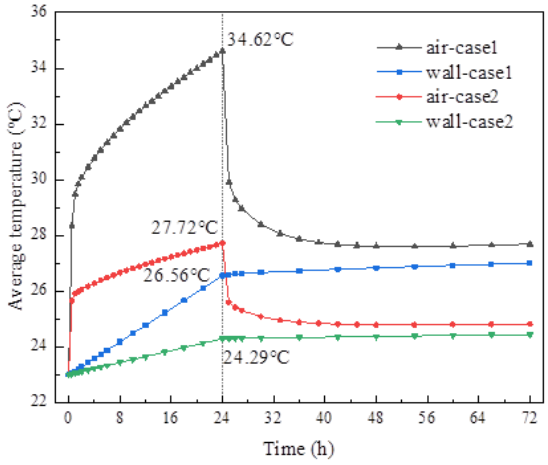

Fig.5. Effect of envelope on indoor air temperature

3.2.2 Unsteady heat transfer in walls

By analyzing the interior of the walls, the overall temperature trend of the walls can be obtained within 0-72 hours, as shown in Fig. 5. Fig. 5 shows the changes in the overall wall temperature over

time for two different operating conditions, case 1 and case 2. It can be seen that within the first 24 hours, the overall wall temperature increases linearly with time for both cases. After 24 hours, although the equipment stops running, the wall temperature does not decrease as rapidly as the air temperature, because heat transfer within the wall occurs primarily through conduction, whereas the air is influenced by convection and radiation, which makes the wall response slower than the air. Under case 1, the wall temperature rises from 23°C to 26.56°C, with a temperature rise of 3.56°C within 24 hours, at a rate of 0.15°C/h. After 24 hours, the overall wall temperature increases slowly due to the cessation of equipment operation, reaching an average temperature of 27°C by 72 hours, with an average temperature rise of 0.44°C within 24-72 hours. Under case 2, the inclusion of ceiling and floor thermal storage enhances the wall's overall thermal storage capacity. In this case, the overall wall temperature rises from 23°C to 24.29°C, with a temperature rise of 1.29°C within 24 hours, at a rate of 0.05°C/h. After 24 hours, the overall wall temperature tends to stabilize, reaching an average temperature of 24.44°C by 72 hours, with an average temperature rise of 0.15°C within 24-72 hours.

To further investigate the temperature field changes inside the wall, case 1, which is closest to the actual operating conditions, was selected as the research object, and the temperature changes of the four walls were analyzed separately to obtain their individual temperature changes over time.

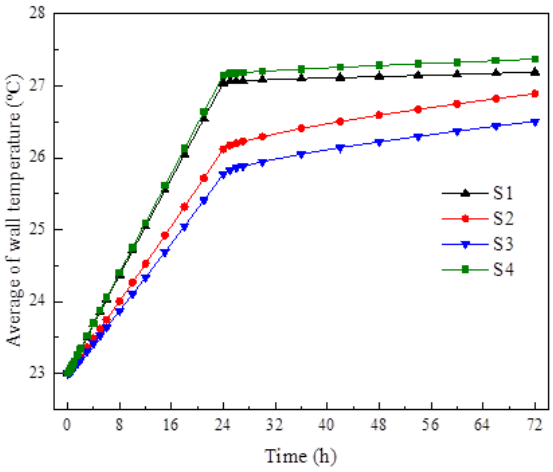

Fig. 6. Average temperature variation of the four walls with time

Fig. 6 shows the variation of the average temperature of the four walls over time, with each wall having a different average temperature. Wall S4 has the largest temperature fluctuation over time, while wall S3 has the smallest temperature fluctuation. This is due to wall S4 being affected by the heat dissipation of the control console and other equipment, resulting in the highest average temperature of the four walls, while wall S1 is most affected by the heat dissipation of the large screen. Compared to walls S1 and S4, there are relatively few devices near walls S2 and S3, resulting in a lower average temperature of the walls. This indicates that the penetration strength of environmental temperature into the walls' internal heat has some impact. From 0 to 24 hours, the temperature rise rate of the wall in the high heat flux density region is higher than that in the low heat flux density region. The temperature rise rate of wall S4 is 0.173°C/h, while wall S3's rise rate is 0.116°C/h. After 24 hours, the temperature of walls S1 and S4 is maintained by the residual heat of the equipment, while walls S2 and S3 are far from the heat source, resulting in a relatively low heat flux density near the walls and a lower temperature rise rate of the walls' average temperature. Within the first 24 hours, wall S3's temperature rise rate is 0.116°C/h. The temperature of wall S3 increases by approximately 0.73°C from 24 to 72 hours.

Fig. 7 displays the time-dependent variation of the surface-averaged temperature at different depths within wall S2. The reference point for this analysis is the interior wall surface in contact with the indoor air, while the outer wall surface serves as the endpoint. The wall is uniformly divided along its thickness, and the surface temperature at each depth is averaged to obtain the temperature variation across the wall's different depths. More specifically, the plot shows the temporal evolution of the

surface-averaged temperature at various depths within wall S2. The averaging process is performed by computing the arithmetic mean of the temperature distribution at each depth, obtained by dividing the wall into uniform intervals along its thickness direction. By this means, the plot enables us to visualize how the temperature varies at different depths within the wall over time.

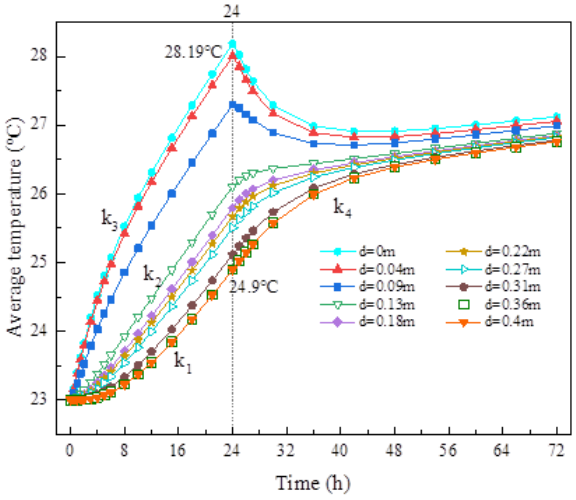

Fig. 7. Temperature variation with time at different depths of the wall

The temperature variation trend displayed in the figure highlights the most significant temperature changes over time at a depth of d = 0m. Table 4 reports the fitting function for the temperature change trend observed within 0-24h, which follows a monotonic increasing trend described by the equation $T = 0.2146\tau + 23.457$, and reaches a maximum temperature of $28.19°C$. Within the depth range of 0m to 0.13m, the wall is highly sensitive to changes in the ambient temperature, and its heat storage capacity is relatively low. As a result, the wall mainly transmits the heat absorbed by the indoor surface to its interior. The temperature at depths less than 0.13m reaches its maximum at 24h, while the magnitude of the temperature peak decreases with increasing depth. Beyond a depth of 0.13m, the peak disappears, and the internal thermal conduction of the wall starts to increase as a function of wall depth. Table.3 also presents the time-dependent variation of the wall temperature at a depth of d = 0.4m, which displays a monotonic increasing trend within 0-72h. The heating rate during the first 24 hours (k_1 = 0.077) is higher than that observed during the subsequent 25-72 hours (k_4 = 0.026).

Table 3 Fitting function of temperature at different depths of the wall against time variation

Wall depth / Time	d =0	d =0.13	d =0.4
0-24h	$T = 0.2146\tau + 23.457$ $R^2 = 0.97$	$T = 0.1328\tau + 22.895$ $R^2 = 0.9985$	$T = 0.0767\tau + 22.796$ $R^2 = 0.9407$
30-72h		$T = 0.0123\tau + 26$ $R^2 = 0.9999$	$T = 0.0257\tau + 25.028$ $R^2 = 0.9024$

During the period of 0-24h, the interior heat flux penetrates the wall to a relatively small distance, resulting in a significant difference in the temperature rise rate of the wall at different depths. The heat transfer from the inner wall is highly affected by the variation in indoor heat flux, but this effect gradually reduces with increasing depth. The fitting model indicates that the increment rate at d = 0m is k3 = 0.215, the temperature rise rate at d = 0.13m is k2 = 0.133, and at d = 0.4m, it is k1 = 0.077.

3.3. Indoor temperature and airflow distribution

3.3.1 Variation of indoor ambient temperature

Based on the numerical simulation results of two cases with and without walls, it was found that walls play a significant role in reducing the temperature in the MCR. To further investigate the impact of personnel positions on the flow and temperature fields within the habitable area under case1 working conditions, an additional standing position for personnel was introduced, as shown in Fig. 2(c). The blue area represents the main activity zone of the personnel, with a heat emission rate of 12kW during the 0-24 hours period, which reduces to 1kW when the equipment is not in operation during the 24-72 hours period. The average indoor temperature was analyzed accordingly.

Fig. 8 presents the temporal variations of indoor air temperature and wall temperature for case 1 and case 3. The trends of the average wall temperature and ambient temperature are similar in both cases. In case 1, the green curve represents the time variation of the average temperature in the MCR from 0-72h, and the red curve shows the time variation of the average temperature of the wall. The temperature

exhibits a monotonically increasing trend in the first 24 hours, with a decreasing rate of increase over time. The indoor ambient temperature increased rapidly by 6.47°C during 0-1 h, with a high rate of increase of 6.47°C/h. After 1h, the trend of indoor ambient temperature changed slowly with time, with a rate of increase of 0.22 °C/h, and the indoor ambient temperature peaked at 34.62 °C at 24h. Due to the heat storage lag of the envelope, the indoor ambient temperature rises faster initially and slows down when the envelope starts to absorb heat. After 24 hours, the indoor temperature starts to decrease as the equipment stops running. At 25h, the indoor ambient temperature drops by 4.71 °C compared with 24h, and the rate of decrease gradually becomes smaller over time until the temperature stabilizes after 48h. The rapid rise in indoor ambient temperature during 0-24h may have some impact on personnel.

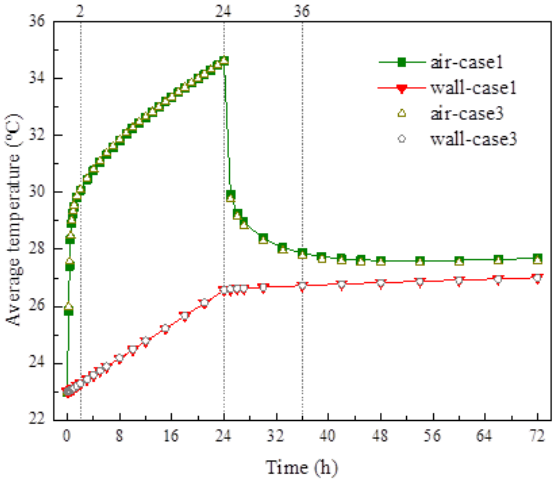

Fig. 8. Indoor ambient temperature and wall temperature change with time

Numerical simulations provide valuable insights into the working conditions of the MCR in a NPP by analyzing the air velocity and temperature distribution. Understanding the airflow distribution within the MCR is critical to maintaining a habitable environment, particularly under accident conditions. In this study, we analyzed the airflow velocity and temperature distribution in the habitable-area of the MCR under case 1 working conditions for a 24-hour period. As shown in Fig.10, the personnel activity area had airflow velocities ranging from 0 to 0.9m/s. The high-speed jet from the air supply outlet resulted in localized areas of higher airflow velocity, while most indoor areas had airflow velocities lower than 0.2m/s.

3.3.2 Indoor air velocity and temperature distribution neat personnel

The cross-sectional positions in Fig.9 (a)-(c) are analyzed to understand the impact of air supply airflow and thermal convection of human heat sources on the airflow distribution. The cross-section in Fig. 10 (a) is located at the rear side of the air supply opening and is not influenced by the air supply airflow. However, the thermal convection generated by human heat sources generates a buoyancy force, causing the airflow to mainly move upward. The cross-section in Fig.9(b) is more affected by the air supply jet. The velocity of the area affected by the air supply jet is significantly higher than the surrounding airflow velocity, with a maximum of 0.9m/s. For the cross-section in Fig.9(c), the impact of the air supply jet is greatly reduced, with a maximum airflow velocity of 0.45 m/s. This is because the airflow ejected from the air supply outlet expands and moves forward, and as the distance increases, there is a lack of inertial force to continue to maintain the horizontal expansion of the airflow, resulting in a smaller airflow velocity. Moreover, higher airflow velocities near the wall can be observed in all three cross-sectional profiles.

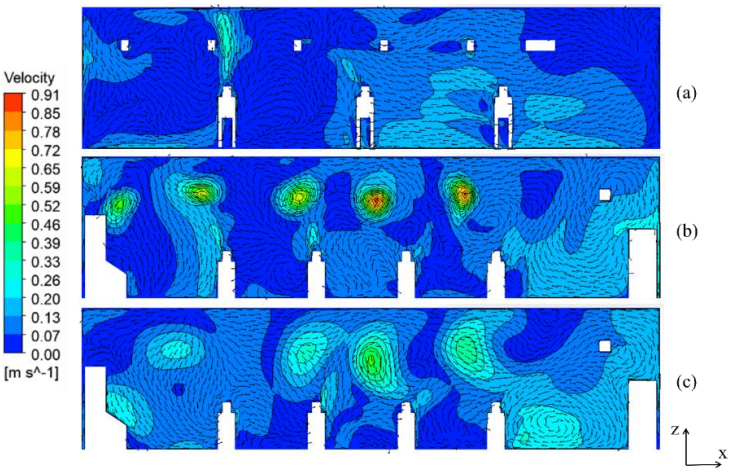

Fig. 9. Velocity distribution of vertical section (a) P1, (b) P2, (c) P3

Based on the data presented in Fig.8, it can be observed that the indoor air temperature exhibited an increasing trend from 0 to 24 hours, reaching its highest point at 24 hours. Subsequently, the temperature gradually decreased from 24 hours to 72 hours, and eventually stabilized after 48 hours. Three time points were selected for analysis, namely 12 hours, 24 hours, and 48 hours, with ambient temperatures of $32.65°C$, $34.62°C$, and $27.61°C$, respectively. Furthermore, information on the temperature distribution in the vicinity of the individuals at these three time points is provided below.

Fig. 10(a), (b), and (c) depict the temperature distribution at three rows of personnel (P1, P2, and P3) at 12, 24, and 48 hours, respectively. The results indicate that the ambient temperature near the personnel in the MCR increased from $31.8°C$ to $33.8°C$ during the 12 hour and 24 hour measurements, which met the requirements for personnel habitability. And at 48 hours, the temperature near the personnel dropped to $27.5°C$.

Furthermore, the indoor air temperature was found to be highest at 24 hours. As the right side of the room had fewer equipment and was located further away from heat sources, the temperature near the right wall was the lowest. In contrast, the left wall had more heat source devices, resulting in a higher temperature compared to the right wall. The airflow in the room was influenced by the heat sources and circulated roughly in a clockwise direction. The airflow on the left side of the room was influenced by thermal convection, resulting in an upward movement of air. Once it reached the ceiling, the air moved horizontally towards the right wall, and finally, returned along the floor, as shown in Fig. 11.

Fig. 2 displays the location of measurement points, which are concentrated in the main activity area of personnel. Meanwhile, Fig. 11 illustrates the trend of air temperature with height at various

locations in the MCR. It can be observed that the temperature near the ceiling is the highest, with a temperature of approximately 35.5°C. This phenomenon is attributed to the upward movement of hot air due to buoyancy force, which concentrates on the ceiling and raises the temperature. Additionally, the temperature on the left side of the MCR is higher than other locations at the same height, such as L7 and L10, because more heat is dissipated from the equipment on the left side, leading to a higher temperature.

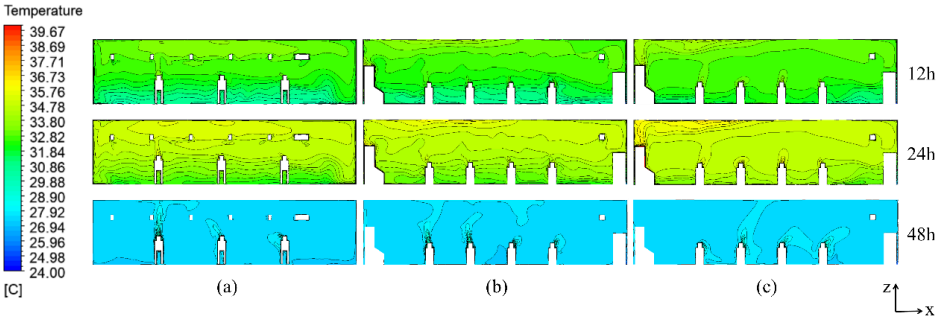

Fig. 10. Temperature distribution in the vertical section of the personnel residence area at different times (a) P1, (b) P2, (c) P3

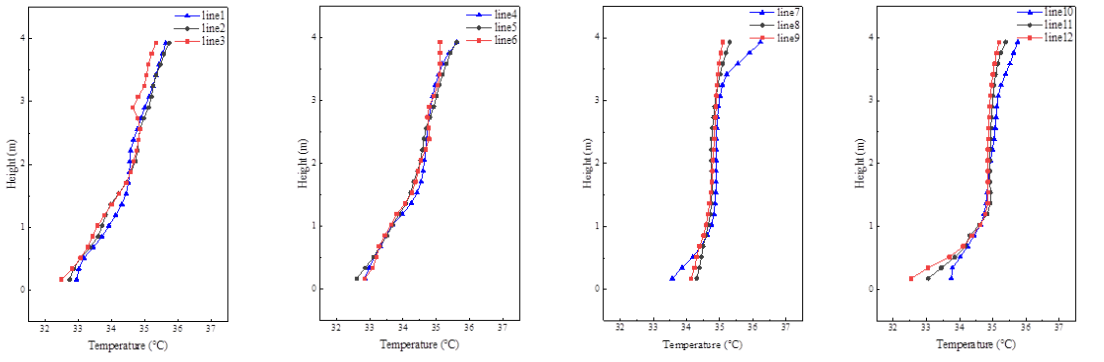

(a) (b) (c) (d)

Fig. 11. Temperature profiles along the height direction

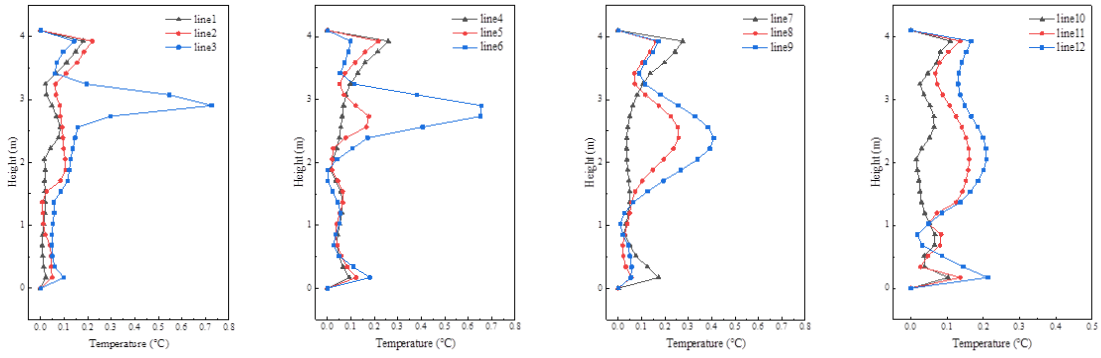

(a) (b) (c) (d)

Fig. 12. Velocity profile along the height direction

Fig.11(a) indicates that line 1 records the highest temperature of 35.6°C at the height position of 3.9 m, demonstrating clear temperature stratification in the cross-section. This phenomenon is caused by lower hot air density, which leads to hot air-driven flow and results in a higher temperature in the

upper part. The velocity vector diagram in Fig. 10 shows that the hot air in the lower part rises upward due to the buoyancy force, supporting the use of the Boussinesq approximation. The temperature distribution in Fig.11(b) resembles that in Fig.11(a), with a visible temperature stratification at this location, where the upper air temperature is higher than the lower air temperature. The vertical temperature rise is $2.7°C$, with a vertical temperature rise rate of $0.72\ °C/m$. In contrast, Fig.11(c) shows that the indoor temperature distribution at this section is relatively uniform, with no stratification. This is due to the equipment's heat dissipation affecting the lower air temperature, resulting in a small difference between the upper and lower air temperatures. Fig.11(d) displays the temperature trend at L10-L12, which is located farther from the air supply and less affected by the jet disturbance. The temperature at L10 is higher than that at L11 and L12, reaching a maximum of $35.75°C$.

Fig. 12 presents the distribution of the airflow field in the MCR, revealing sudden velocity change points influenced by the air supply jet. The mutation point on L6 records the highest velocity of 0.66m/s due to the air supply jet passing through L6's location. The jet's movement is propelled forward by the inertial force, which gradually decreases with distance. As a result, the highest velocity point's height decreases from 2.9m in Fig. 12(b) to nearly 2m in Fig. 12(d).

Fig. 12(a), (b), and (c) are significantly affected by the air supply jet, resulting in large local forced convection. However, the personnel activity area is primarily concentrated below 2m. There are no sudden velocity change points in the area below 2m, and the airflow distribution is relatively uniform. Consequently, the air supply jet has little impact on personnel. The average wind speed calculated in the area below 2m, excluding the near wall, is 0.07m/s. The perceived wind strength is not very strong, meeting the requirements of the "Design Code for Heating, Ventilation and Air Conditioning in Civil Buildings."

3.4. CO_2 concentration field

The concentration of CO_2 in a room is primarily influenced by the number of occupants (individuals or residents within a building) and their metabolic activity. In the control room, the number of occupants is fixed at 11 people, therefore the CO_2 concentration is mainly determined by human metabolism. Fig.13 shows that the indoor CO_2 concentration trends are similar in case 1 and case 3, but the CO_2 concentration in case 3 is lower than in case 1. In both cases, the average CO_2 concentration in the control room exceeds 800 ppm after 3.5 hours and reaches over 1000 ppm after 6 hours. Subsequently, the CO_2 concentration continues to rise and stabilizes gradually after 30 hours. In case 1, the average CO_2 concentration stabilizes between 1560 ppm and 1590 ppm, while in case 3, the average CO_2 concentration stabilizes between 1500 ppm and 1530 ppm. Therefore, the average CO_2 concentration in case 1 is 70 ppm higher than in case 3.

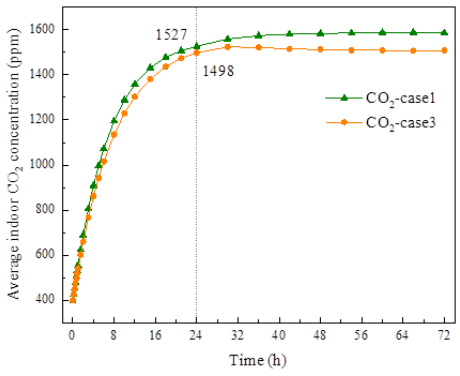

Fig. 13 Temporal variations in average indoor CO2 concentration

Fig.14 presents contour plots of the CO_2 concentration under two cases, revealing the uneven distribution of indoor CO_2 concentration over a 24-hour period. In case 1, the difference between the minimum and maximum CO_2 concentrations is about 29 ppm, with a minimum concentration of 1515

ppm and a maximum concentration of 1544 ppm. The CO_2 concentration on the left side is lower than on the right side, which may be due to the limited supply of fresh air, leading to a CO_2 peak in the middle of the first row of occupants. In case 3, the difference between the minimum and maximum CO_2 concentrations is also about 29 ppm, with a minimum concentration of 1486 ppm and a maximum concentration of 1516 ppm. The CO_2 concentration on the left side is higher than on the right side, which may be due to the occupants gathering together, resulting in a relatively lower CO_2 concentration in front of the control room. Despite the maximum level of CO_2 exhaled by the occupants being set, the results indicate that the CO_2 concentrations in all areas meet the requirements for habitability.

3.5. The impact of personnel position

Based on the comparison of the two working conditions in Fig.8, it can be observed that there is little difference in the indoor temperature change trend, with a nearly constant temperature at each time point. However, the first row of personnel in case1 was found to be located in a relatively high-temperature area, as shown in Fig.2. To improve the indoor thermal comfort, the position of personnel was optimized by moving the first row of personnel to the back of the relatively low-temperature area. The impact of the optimized personnel station on the indoor thermal environment was investigated by comparing the habitable-area before and after the change. Significant changes in the average temperature and velocity were observed, as shown in Fig. 15(a) and 15(b), respectively.

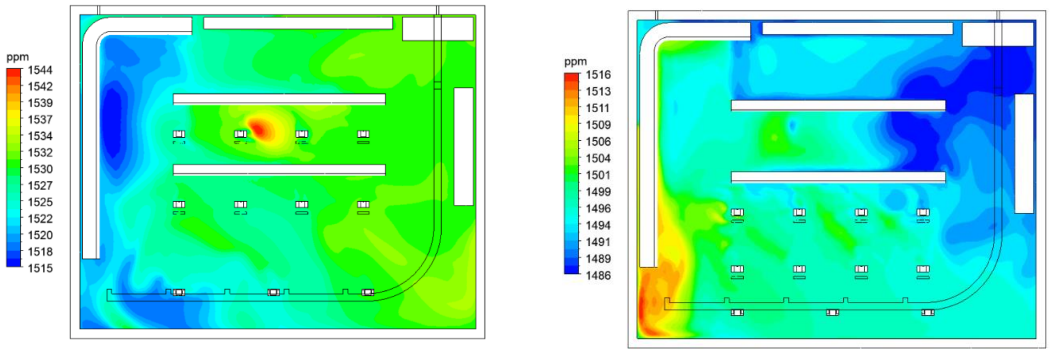

(a)case1 (b)case3

Fig.14 Contours of the CO2 concentration (ppm) on the horizontal plan z=1m

Fig. 15(a) presents the average temperature variation in the space below 2.2 m in the main personnel activity area for both case1 and case3, before and after the personnel station optimization. The results showed that the indoor temperature increases with height in both cases. However, after optimizing the personnel station, the average temperature of the personnel activity area decreased by $0.42°C$ compared to case1. This improvement can be attributed to the better distribution of the heat sources after moving the first row of personnel to a relatively cooler area.

Furthermore, Fig. 15(b) shows the comparison of the average velocity before and after the optimized personnel station. It can be observed that the average velocity in both case1 and case3 was maintained below 0.2 m/s, and the average velocity in case3 was lower than that in case1. This can be attributed to the weakened influence of the air supply jet after the personnel moved to the back row, resulting in lower wind speeds. The optimized personnel station not only improves the thermal comfort of the indoor environment but also reduces the air velocity in the personnel activity area, which is beneficial for meeting the requirements of habitability.

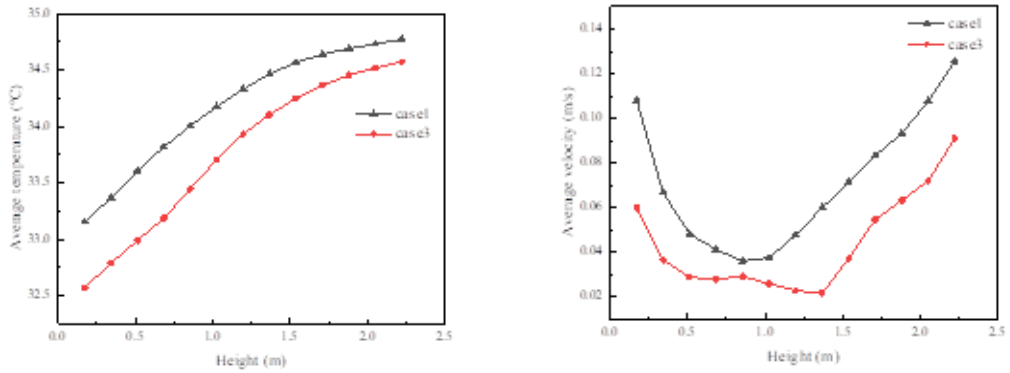

(a) (b)

Fig.15. Comparison of average temperature and average speed of habitable-area in two cases

This study conducted an in-depth investigation into the influence of the average CO_2 concentration in the habitable-area with height change under two working conditions Fig.16 shows that the average CO_2 concentration in the habitable-area under case 1 is higher than that under case 3, with a difference of 30 ppm on average. This indicates that the location of personnel has a certain impact on

the distribution of indoor CO_2 concentration. Additionally, this study found that indoor CO_2 concentration gradually increases with height, which is most evident under case 3. The CO_2 concentration below 1m is 1495 ppm, and it starts to increase above 1m, reaching 1530 ppm at 2m, an increase of 35 ppm. The reason for this phenomenon is that under case 3, people are concentrated in certain locations, and CO_2 exhaled and moves upward with the hot air, leading to a higher concentration of CO_2 at higher locations. In contrast, in case 1, due to the dispersion of personnel, the CO_2 concentration varies more uniformly with height. Additionally, this study found that under both working conditions, the CO_2 concentration in all areas is below the habitable requirements, indicating that the current ventilation system has a good effect on maintaining indoor air quality. This result provides an important reference for the design and optimization of indoor environments.

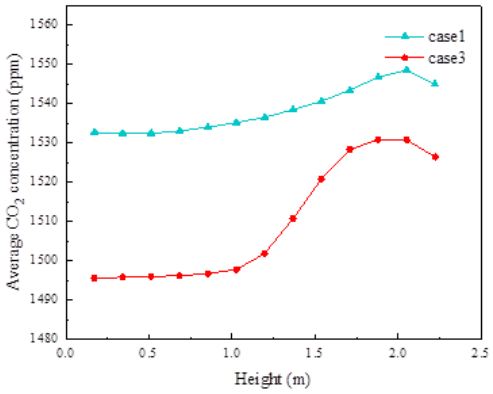

Fig. 6 Comparison of average CO2 concentration of habitable-area in two cases

4. Conclusions

In this paper, the airflow organization in the MCR of a nuclear power plant was studied by numerical simulation using CFD method, as well as the thermal conduction characteristic of the MCR enclosure under unsteady conditions. The simulation results show that:

(a) The control room walls play a crucial role in reducing indoor air temperature during the entire power outage scenario in the nuclear power plant. Without these walls, the indoor temperature would rapidly increase within a short period, surpassing the maximum allowable temperature for habitability requirements, thus failing to meet the habitability standards indoors.

(b) The heat storage capacity and fresh air supply of the main control room (MCR) enclosure structure can meet the habitability requirements of the MCR under certain conditions. For example, in Case 1, the temperature rise in the MCR over 24 hours is 11.62°C, resulting in an indoor environment temperature of approximately 34.62°C, which meets habitability requirements.

(c) The thermal storage analysis of the walls indicates that the thermal storage performance is influenced by the heat flux density, with the temperature rise rate of walls in high heat flux density areas greater than those in low heat flux density areas. Therefore, the temperature rise rates of walls S1 and S4, located near the heat-generating equipment, are higher than those of walls S2 and S3. In particular, internal heat transfer analysis of wall S2 reveals that the temperature rise rates at d = 0m, d = 0.13m, and d = 0.4m are 0.215, 0.133, and 0.077, respectively. This indicates that the influence of internal heat flux on the wall decreases gradually with increasing depth.

(d) Analysis of the temperature and velocity fields near the indoor personnel reveals higher temperatures near the heat sources, potentially causing discomfort to individuals. Therefore, optimizations were made to the positioning of personnel. Following optimization, the temperature in the personnel activity area decreased by 0.42°C, and the average indoor CO2 concentration decreased by 30ppm. Consequently, optimization adjustments can be made to the working area of personnel in the control room. The findings of this study provide valuable insights for the design and optimization of indoor environments in similar scenarios.

Nomenclature

CFD	computational fluid dynamic	Re	Reynolds number (=*UD/n*), [-]
d	hydraulic diameter [m]	T	temperature [$°C$]
e	energy per unit mass [Jkg-1]	V	volume [m3]
g	gravitational acceleration [ms-2]	$\vec{v}$	the fluid velocity vector [ms-1]
		z	vertical coordinate [m]
h	specific enthalpy [Jkg-1]	Greek symbols	
I	Turbulence intensity [-]	β	thermal expansion coefficient [K-1]
k	thermal conductivity [Wm-1K-1]	ε	turbulence dissipation [m2s-3]
		ε_k	emissivity
MCR	main control room	μ	dynamic viscosity [kgm-1s-1]
p	pressure [Pa]		

References

[1] P. Liu, P. Chu, and J. Hou, "Accommodation issue of nuclear power in China: Status quo, barriers and solutions," *Energy Strategy Rev.*, vol. 22, pp. 166–178, Nov. 2018, doi: 10.1016/j.esr.2018.08.005.

[2] Y.-C. Chang and Y. Zhao, "The Fukushima Nuclear Power Station incident and marine pollution," *Mar. Pollut. Bull.*, vol. 64, no. 5, pp. 897–901, May 2012, doi: 10.1016/j.marpolbul.2012.01.038.

[3] E. Hollnagel, "THE FUKUSHIMA DISASTER – SYSTEMIC FAILURES AS THE LACK OF RESILIENCE," *Nucl. Eng. Technol.*, p. 8, 2013.

[4] J. A. Orosa and A. C. Oliveira, “A field study on building inertia and its effects on indoor thermal environment,” *Renew. Energy*, vol. 37, no. 1, pp. 89–96, Jan. 2012, doi: 10.1016/j.renene.2011.06.009.

[5] International Nuclear Safety Advisory Group and International Atomic Energy Agency, Eds., *Basic safety principles for nuclear power plants: 75-INSAG-3 Rev. 1*, Rev. Vienna: International Atomic Energy Agency, 1999.

[6] Zheng, G., Zhao X., 2013. Optimization of the main control room habitability system in nuclear power plant. China Nuclear Power, 6, 291–295. (in Chinese)

[7] Zhang, G., Wang, C., 2017. Emergency habitability system for main control room of AP1000 third generation nuclear power plant. HV&AC, 47, 32-35. (in Chinese)

[8] H. Li, K. Li, B. Liu, J. Li, Q. Meng, and C. Yang, “Study on the passive refrigeration for main control room of nuclear power plant in power outage accident,” *Nucl. Eng. Des.*, vol. 326, pp. 183–189, Jan. 2018, doi: 10.1016/j.nucengdes.2017.11.022.

[9] Zheng, S., Xu, N., 2010. The study on the test of the track of the dynamic cooling load of the DVC system. Energy Conservation technology, 28, 424-426. (in Chinese)

[10] F. M. Abed, O. K. Ahmed, and A. E. Ahmed, “Effect of climate and design parameters on the temperature distribution of a room,” *J. Build. Eng.*, vol. 17, pp. 115–124, May 2018, doi: 10.1016/j.jobe.2018.02.007.

[11] “NB⁄T 20395-2017- Residential Design Requirements for the Control Room.pdf.” https://max.book118.com/html/2019/0613/7060054031002033.shtm (accessed Jun. 07, 2022).

[12] P. Wouters, D. Ducarme, J. Demeester, and L. Vandaele, “Ventilation requirements in non-domestic buildings and energy efficiency,” p. 5.

[13] T. L. Schulz, “Westinghouse AP1000 advanced passive plant,” *Nucl. Eng. Des.*, vol. 236, no. 14–16, pp. 1547–1557, Aug. 2006, doi: 10.1016/j.nucengdes.2006.03.049.

[14] Y. Jia, Y. Liu, S. Sun, H. Li, and L. Jiao, “Refrigerating characteristics of ice storage capsule for temperature control of coal mine refuge chamber,” *Appl. Therm. Eng.*, vol. 75, pp. 756–762, Jan. 2015, doi: 10.1016/j.applthermaleng.2014.10.036.

[15] S. Wang, G. Chen, M. Fang, and Q. Wang, “A new compressed air energy storage refrigeration system,” *Energy Convers. Manag.*, vol. 47, no. 18–19, pp. 3408–3416, Nov. 2006, doi: 10.1016/j.enconman.2006.01.007.

[16] F. R. Siddiqui, M. A. I. El-Shaarawi, and S. A. M. Said, “Exergo-economic analysis of a solar driven hybrid storage absorption refrigeration cycle,” *Energy Convers. Manag.*, vol. 80, pp. 165–172, Apr. 2014, doi: 10.1016/j.enconman.2014.01.029.

[17] B. Sutharshan, M. Mutyala, R. P. Vijuk, and A. Mishra, “The AP1000TM Reactor: Passive Safety and Modular Design,” *Energy Procedia*, vol. 7, pp. 293–302, 2011, doi: 10.1016/j.egypro.2011.06.038.

[18] Y. Huang, X. Su, X. Wu, W. Ye, and X. Zhang, “Dynamic thermal performance analysis for fin-concrete ceiling in main control rooms of passive nuclear power plants,” *Case Stud. Therm. Eng.*, vol. 28, p. 101402, Dec. 2021, doi: 10.1016/j.csite.2021.101402.

[19] L. S. Al-Rukaibawi, Z. Szalay, and G. Károlyi, “Numerical simulation of the effect of bamboo composite building envelope on summer overheating problem,” *Case Stud. Therm. Eng.*, vol. 28, p. 101516, Dec. 2021, doi: 10.1016/j.csite.2021.101516.

[20] L. N. Gollapudi, R. Senanayake, C. Georgantopoulou, and A. K. Singh, “Numerical heat transfer analysis of a thermal energy storage system enclosure with horizontal fin for sustainable energy storage,” *Case Stud. Therm. Eng.*, vol. 28, p. 101670, Dec. 2021, doi: 10.1016/j.csite.2021.101670.

[21] A. Jahanbin and E. Zanchini, “Effects of position and temperature-gradient direction on the performance of a thin plane radiator,” *Appl. Therm. Eng.*, vol. 105, pp. 467–473, Jul. 2016, doi: 10.1016/j.applthermaleng.2016.03.018.

[22] D. Palanisamy and B. K. Ayalur, “Development and testing of condensate assisted pre-cooling unit for improved indoor air quality in a computer laboratory,” *Build. Environ.*, vol. 163, p. 106321, Oct. 2019, doi: 10.1016/j.buildenv.2019.106321.

Paper submitted: 19.01.2024

Paper revised: 09.03.2024

Paper accepted: 14.03.2024